catalysts

MDPI

Article

Halloysite@Polydopamine Nanoplatform for Ultrasmall Pd and Cu Nanoparticles: Suitable Catalysts for Hydrogenation and Reduction Reactions

Marina Massaro [1], Chiara D'Acunzi [2], Stefano Paganelli [2,3,*], Maria Laura Alfieri [4], Leonarda F. Liotta [5], Alberto Lopez-Galindo [6], Raquel de Melo Barbosa [7], Oreste Piccolo [8], Rita Sánchez-Espejo [7], César Viseras [6,7] and Serena Riela [9,*]

1 Dipartimento di Scienze e Tecnologie Biologiche, Chimiche e Farmaceutiche (STEBICEF), Università di Palermo, Viale delle Scienze, Parco d'Orleans II, Ed. 17, 90128 Palermo, Italy; marina.massaro@unipa.it
2 Dipartimento di Scienze Molecolari e Nanosistemi, Università Ca' Foscari Venezia, Via Torino 155, 30172 Venezia Mestre (VE), Italy; dac.chiara@hotmail.it
3 Consorzio Interuniversitario Reattività Chimica e Catalisi (CIRCC), Via Celso Ulpiani 27, 70126 Bari, Italy
4 Dipartimento di Scienze Chimiche, Università di Napoli Federico II, Via Cinthia 4, 80126 Napoli, Italy; marialaura.alfieri@unina.it
5 Istituto per lo Studio dei Materiali Nanostrutturati (ISMN)-CNR, Via Ugo La Malfa 153, 90146 Palermo, Italy; leonarda.liotta@ismn.cnr.it
6 Andalusian Institute of Earth Sciences (IACT), Consejo Superior de Investigaciones Científicas, 18100 Armilla, Spain; alberto.lopez@csic.es (A.L.-G.); cviseras@ugr.es (C.V.)
7 Department of Pharmacy and Pharmaceutical Technology, Faculty of Pharmacy, University of Granada, Campus Universitario de Cartuja, 18071 Granada, Spain; rbarbosa@ugr.es (R.d.M.B.); ritamsanchez@ugr.es (R.S.-E.)
8 Studio di Consulenza Scientifica (SCSOP), Viale Trieste 35, 53100 Siena, Italy; orestepiccolo@tin.it
9 Dipartimento di Scienze Chimiche (DSC), Università di Catania, Viale Andrea Doria 6, 95125 Catania, Italy
* Correspondence: spag@unive.it (S.P.); serena.riela@unict.it (S.R.)

Academic Editor: Mário Manuel Quialheiro Simões

Received: 15 October 2025
Revised: 24 October 2025
Accepted: 27 October 2025
Published: 1 November 2025

Citation: Massaro, M.; D'Acunzi, C.; Paganelli, S.; Alfieri, M.L.; Liotta, L.F.; Lopez-Galindo, A.; de Melo Barbosa, R.; Piccolo, O.; Sánchez-Espejo, R.; Viseras, C.; et al. Halloysite@Polydopamine Nanoplatform for Ultrasmall Pd and Cu Nanoparticles: Suitable Catalysts for Hydrogenation and Reduction Reactions. *Catalysts* **2025**, *15*, 1029. https://doi.org/10.3390/catal15111029

Abstract

The design of sustainable nanomaterials for catalysis is a key challenge in green chemistry. Herein, we report the synthesis of halloysite nanotube (Hal)-based nanomaterials selectively functionalized with a bio-inspired polydopamine (PDA) coating, which enables the controlled anchoring of palladium and copper nanoparticles (PdNPs and CuNPs). This mild and ecofriendly strategy yields highly dispersed and ultrasmall (<5 nm) metal nanoparticles without the need for surfactants or harsh reagents. The resulting materials, Hal@PDA/PdNPs and Hal@PDA/CuNPs, were evaluated in two well-established model reactions commonly employed to probe catalytic performance: cinnamaldehyde hydrogenation and 4-nitrophenol reduction. Hal@PDA/PdNPs displayed complete conversion and >90% selectivity toward hydrocinnamaldehyde at low Pd loading (0.8 wt%) and maintained its efficiency over six catalytic cycles (TOF up to 0.1 s^{-1}), while Hal@PDA/CuNPs retained high activity through eight consecutive runs in the reduction of 4-nitrophenol. Hal@PDA/CuNPs proved to be an excellent recyclable catalyst for the reduction of 4-nitrophenol, retaining high activity through eight consecutive runs. Overall, this study introduces a robust and modular approach to fabricating halloysite-based nanocatalysts, demonstrating their potential as green platforms for metal nanoparticle-mediated transformation.

Keywords: halloysite; polydopamine; heterogeneous catalyst; hydrogenation reaction; reduction reaction

1. Introduction

The shift toward more sustainable and environmentally friendly catalytic systems has sparked a growing interest in the use of naturally abundant, low-cost materials as functional supports for metal nanoparticles [1]. Clay minerals are invaluable resources in material science, offering unique properties and cost-effective availability [2]. Among them, halloysite (Hal), a member of the kaolin group, stands out due to its distinctive hollow tubular structure and chemical versatility. This naturally abundant aluminosilicate mineral, with the formula $Al_2Si_2O_5(OH)_4 \cdot nH_2O$, features siloxane groups on its outer surface and aluminol groups within its lumen. The distinct chemical nature of these surfaces allows for selective functionalization, making halloysite an exceptional candidate for advanced material applications [3]. The ability to modify halloysite's surfaces through targeted functionalization has unlocked a plethora of possibilities in fields such as catalysis [4–8], drug delivery, and environmental remediation [9]. In particular, the use of halloysite for catalytic purposes is a very promising strategy for stabilizing metal nanoparticles of small dimensions that can be reused for several consecutive runs without loss of catalytic activity [10,11].

Among various strategies, polymer-based functionalization has gained significant attention. Polydopamine (PDA), a bio-inspired eumelanin-like polymer rich in functional groups (e.g., hydroxyl, amine, and carboxyl), has emerged as a versatile coating material [12,13]. It provides a platform for immobilizing and stabilizing metal nanoparticles, further broadening the halloysite's potential for application as a heterogeneous support material. In this context, for example, Hal coated with PDA was used for the immobilization of Fe^{2+} ions, and the obtained material was successfully utilized as a catalyst for the Fenton reaction to remove organic dyes [14]. Metal nanoparticles (NPs), particularly those based on Pd and Cu, are widely used in catalysis due to their high surface-to-volume ratio and excellent activity. However, their application is often limited by issues related to aggregation, leaching, or sintering. A key challenge is still the design of effective supports that ensure strong metal–support interaction and long-term stability [15].

In this study, we employ a site-specific PDA coating strategy, enabled by predecoration of Hal with ZnO nanoparticles [16] to create a robust Hal@PDA [17] nanoplatform for anchoring Pd and Cu nanoparticles. This approach leverages the basicity of ZnO nanoparticles anchored onto the halloysite surface to induce dopamine polymerization under mild conditions, avoiding bulk polymer precipitation [16]. Compared to traditional dip-coating methods, this strategy offers a cleaner, more controlled synthesis process, enhancing material stability. In addition, the presence of site-specific PDA coating onto Hal external surface could ensure the stabilization of metal nanoparticles with small and uniform size, which could be beneficial for catalytic purposes. The synthesized Hal@PDA/PdNP and Hal@PDA/CuNP materials were thoroughly characterized by several techniques and tested in two model catalytic reactions: (i) the hydrogenation of (E)-cinnamaldehyde, in the presence of isopropanol using a substrate/MNP molar ratio of 1000/1 at 50 °C, varying reaction time and H_2 pressure; (ii) the reduction of 4-nitrophenol.

The two systems demonstrated complementary catalytic behavior: Hal@PDA/PdNPs exhibited high activity, selectivity, and recyclability in the hydrogenation of cinnamaldehyde, whereas Hal@PDA/CuNPs outperformed in the reduction of 4-nitrophenol. These results underline the versatility of the Hal@PDA architecture in stabilizing metal nanoparticles and tailoring their reactivity toward specific transformations. By combining selective surface functionalization with efficient nanoparticle anchoring, this study highlights the potential of Hal@PDA as a robust and tunable nanoplatform for the design of next-generation heterogeneous catalysts.

2. Results and Discussion

2.1. Synthesis and Characterization of the Hal@PDA/Supported Metal Nanoparticles

The hybrid materials were synthesized through a two-step procedure, as reported in Figure 1. Firstly, the site-specific functionalization of the halloysite external surface by polydopamine was carried out as previously reported [17]. In brief, Hal was decorated with ZnONPs [16] with basic properties, affording the Hal@ZnO nanomaterial that was used as a scaffold to induce the surface-specific polymerization and deposition of dopamine coatings at a relatively low pH (6.5) under conditions hindering polymer precipitation in the bulk mixture [17]. As previously reported, the characterization of the nanomaterial showed that by adopting this strategy, a polydopamine coating onto the basic sites, provided by the ZnO nanoparticles anchored onto the Hal surface, occurs, with a thickness of ca. 1 nm [17]. This coating proves to be stable and does not desorb under normal conditions, as its removal occurs only in an alkaline environment combined with hydrogen peroxide.

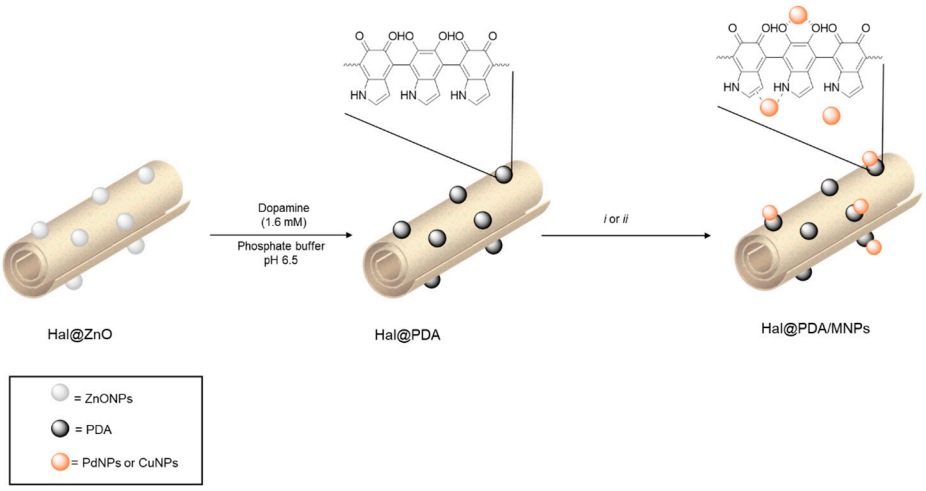

Figure 1. Schematic representation of the synthesis of Hal@PDA/MNP nanomaterials obtained. Step (1) site-specific PDA coating of Hal@ZnO under mild aqueous conditions (pH 6.5). Step (2) separate metal loading routes: (*i*) Hal@PDA/CuNPs: $CuCl_2$, H_2O, 25 °C, 16 h, followed by $NaBH_4$, EtOH, 25 °C, 6 h; (*ii*) Hal@PDA/PdNPs: $PdCl_2$, NaCl, H_2O, 25 °C, 16 h, followed by $NaBH_4$, EtOH, 25 °C, 6 h.

The obtained Hal@PDA nanomaterial was then dispersed in water in the presence of Na_2PdCl_4 or $CuCl_2$, followed by reduction with $NaBH_4$ in ethanol leading to the final metal-based catalyst Hal@PDA/MNPs (Hal@PDA/PdNPs or Hal@PDA/CuNPs), affording nanomaterials with a metal content of a maximum of 3.6 and 0.62 wt% for Pd and Cu, respectively (see infra). Both catalysts have been characterized by means of TGA, XRD, XPS, and TEM.

It should be noted that TGA analysis carried out under air flow was shown to be a very useful technique for the exact quantification of the Cu and Pd metal content. In Figure 2a, the TGA curve of the starting Hal@PDA nanomaterial is compared with those of the Cu- and Pd-loaded samples. All curves show the typical mass loss of halloysite due to the removal of differently bonded water molecules, from the surface (100–300 °C) to the interlayer structure at higher temperatures, between ~300 and 500 °C [18]. In the same range of temperature, the decomposition of the PDA polymer likely occurs [17].

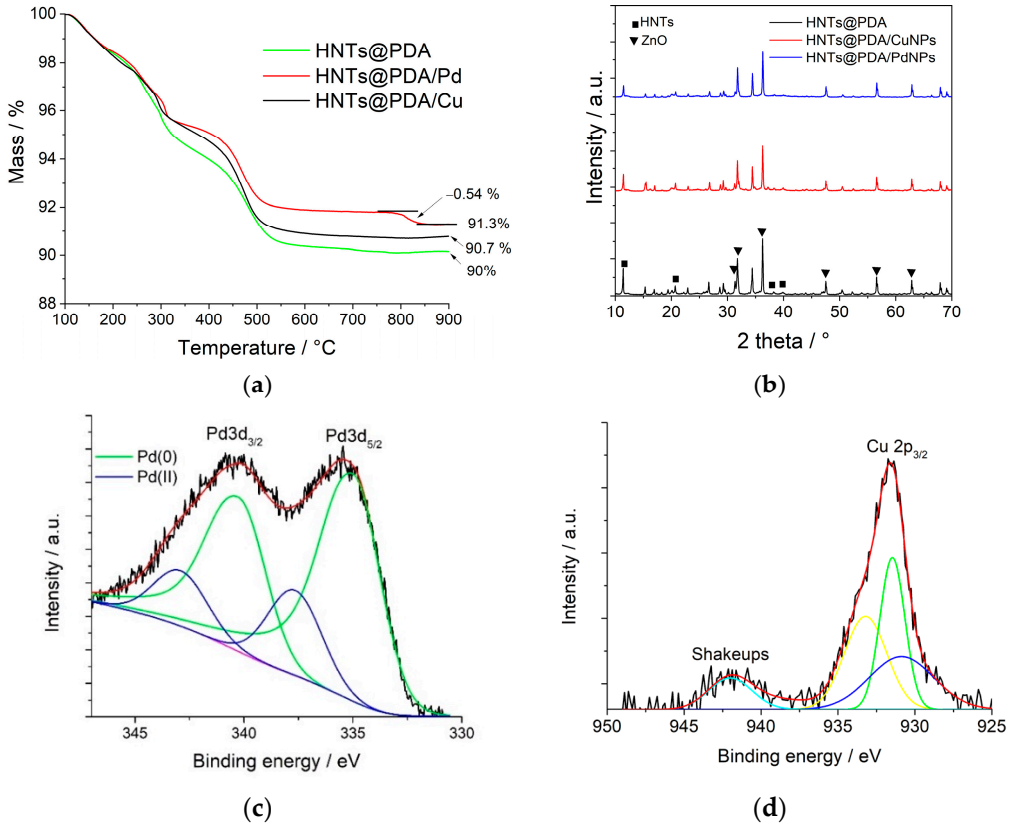

Figure 2. (**a**) Thermogravimetric curves; (**b**) XRD spectra of Hal@PDA, Hal@PDA/PdNP, and Hal@PDA/CuNP nanomaterials; and (**c**,**d**) high-resolution X-ray photoelectron spectroscopy (XPS) of (**c**) Hal@PDA/PdNP and (**d**) Hal@PDA/CuNP nanomaterials.

According to the literature [19,20], the TG curve registered for the Hal@PDA/CuNP sample takes into account the formation of Cu_2O during the treatment under air flow, along with the occurrence of the previously discussed halloysite modification and PDA oxidation. Therefore, based on the final mass value of 90% achieved at 1000 °C, a loading of Cu_2O equal to 0.7 wt% was estimated (90.7–90%), corresponding to 0.62 wt% of Cu. For the Hal@PDA/PdNP sample, based on the weight loss at around 800 °C equal to 0.54% corresponding to the decomposition of PdO (formed under oxidizing conditions) to metallic Pd, giving rise to O_2 evolution [21], a Pd loading of 3.6 wt% was calculated.

In Figure 2b, the XRD spectra of Hal@PDA, Hal@PDA/PdNP, and Hal@PDA/CuNP nanomaterials are shown. All nanomaterials showed the typical reflections of Hal [22], namely, the reflections at 2θ 12°, 20°, 25°, 35°, 54°, and 62° corresponding to the planes (001), (100), (002), (100), (210), and (300), respectively, matching with the JCPD card no. 00–029-1487. In addition to these, the XRD pattern of the Hal@PDA nanomaterial shows the reflection attributable to ZnONPs with wurtzite phase [23], also observable in the XPS survey (Figure S5). The XRD spectra of the Hal@PDA/PdNP and Hal@PDA/CuNP nanomaterials did not show any significant diffraction peaks attributable to the metal nanoparticles. It is well recognized that the XRD technique has limitations based on particle size; therefore, it is hypothesized that metal nanoparticles with a size smaller than 5 nm were obtained, resulting in no measurable signal [24].

Figure 2c,d show the XPS spectra of the Hal@PDA/PdNP and Hal@PDA/CuNP nanomaterials. As can be seen, the Pd3d spectrum (Figure 2c) shows the presence of two doublets due to typical spin–orbit splitting ($Pd3d_{5/2}$ and $Pd3d_{3/2}$ components) and the concomitant presence of two species of palladium, namely, Pd(0) and Pd(II). The relative

amount of the components due to Pd(0) and Pd(II) species allowed us to estimate a degree of reduction of ca. 78%.

Similarly, the high–resolution Cu 2p spectrum of Hal@PDA/CuNPs (Figure 2d) shows the Cu $2p_{3/2}$ peak at ca. 931 eV that is deconvoluted in three main peaks. The peaks with a lower binding energy, at ~931 eV, were assigned to Cu^{+}/Cu^{0}, considering that Cu^{+} and Cu^{0} possessed similar peak positions [25]. However, since it is known that the Cu(I) peak is broader compared to that of metallic Cu, it could be hypothesized that the peak centered at 930.87 eV is related to the Cu(I) species, while the one at 931.46 eV is related to Cu(0), respectively.

The other Cu 2p3/2 peak at ~934.6 eV was associated with the Cu^{2+} state. The satellite peak at 942 eV is attributed to the ligand-to-metal charge transfer that distinctly specifies the existence of Cu^{2+} species [26].

The morphology of the Hal@PDA/PdNP and Hal@PDA/CuNP nanomaterials was imaged by transmission electron microscopy (TEM), which showed the typical tubular structure of halloysite (Figure 3A) and the presence of Pd nanoparticles selectively distributed on the polydopamine spots on the Hal surface, as highlighted by the elemental mapping extrapolated by energy X-ray spectroscopy (Figure 3B). Fast Fourier transform on high-magnification HR-TEM showed nanocrystalline Pd nanoparticles with a *d* spacing of 0.23 nm, corresponding to the (111) of planes of face-centered cubic (fcc) Pd [27] (Figure 3C). The EDX spectrum on a selected area showed the presence of the Pd atoms beside the Al, Si, O, C, and Zn ones related to the support (Figure 3D). From statistical analysis, the Hal@PDA/PdNP nanomaterial showed the presence of small Pd nanoparticles with an average diameter of 3.8 ± 0.6 nm and a narrow size distribution (Figure 3E).

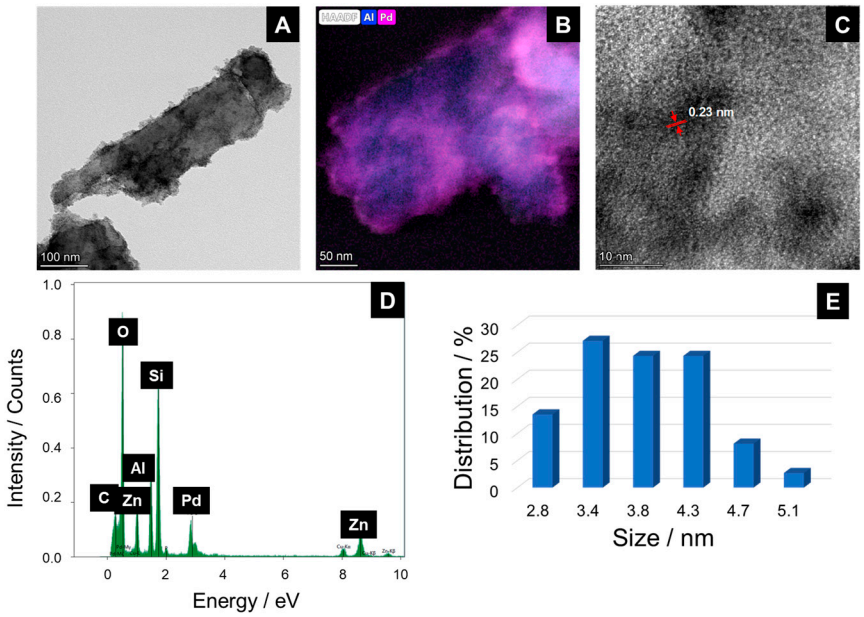

Figure 3. (**A**) TEM image; (**B**) EDX elemental mapping images; (**C**) HR-TEM image of the Hal@PDA/Pd nanomaterial; (**D**) EDS analysis on a selected area; (**E**) Hal@PDA/PdNP diameter size distribution (number of counts = 80).

Similar considerations can be made for the Hal@PDA/CuNP nanomaterial; in this case, HR-TEM investigations showed the presence of Cu nanoparticles with a *d* spacing of 0.22 nm corresponding to the (111) of planes of face-centered cubic (fcc) Cu (Figure 4B). From statistical analysis, the Hal@PDA/Cu nanomaterial showed the presence of small Cu nanoparticles with an average diameter of 4.9 ± 1.3 nm and narrow size distribution (Figure 4C).

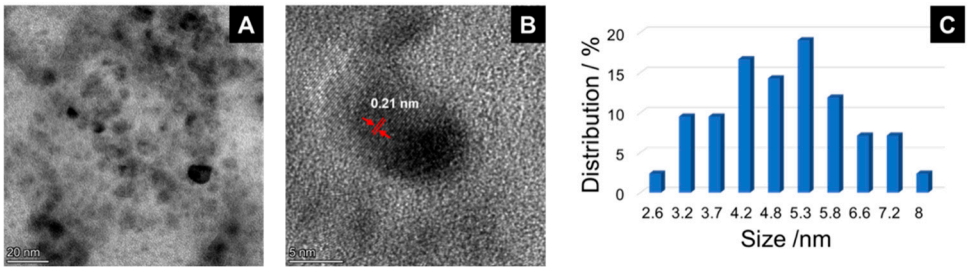

Figure 4. (**A**,**B**) HR-TEM image of the Hal@PDA/CuNP nanomaterial; (**C**) Hal@PDA/CuNP diameter size distribution (number of counts = 80).

These results further underscore the crucial role of the site-specific PDA coating strategy in defining the structure and performance of the final Hal@PDA/MNP nanomaterials. In particular, ZnONPs-assisted polymerization enables the selective formation of a thin PDA layer on the outer surface of halloysite, preventing bulk polymerization and internal lumen blockage. This controlled coating provides a homogeneous and stable interface that allows the uniform dispersion and tight anchoring of ultrasmall Pd (3.8 ± 0.6 nm) and Cu (4.9 ± 1.3 nm) nanoparticles, in contrast with conventional PDA deposition methods that often result in non-uniform coverage and lumen obstruction, as previously reported for Tris-buffer polymerization routes by Sahiner et al. [28].

2.2. Catalytic Experiments

To evaluate the functional performance of the Hal@PDA-supported metal nanoparticles, two well-established model reactions were selected: the hydrogenation of (E)-cinnamaldehyde and the reduction of 4-nitrophenol.

2.2.1. Cinnamaldehyde Hydrogenation

The hydrogenation of cinnamaldehyde is a pivotal reaction in the chemical industry, producing a range of valuable intermediates used in the manufacture of fine chemicals, pharmaceuticals, fragrances, and flavorings [29]. The challenge in the hydrogenation process lies in achieving high selectivity toward the desired product while maintaining efficiency and minimizing by-products. Therefore, to evaluate the catalytic activity and selectivity of the Hal@PDA/PdNP and Hal@PDA/CuNP nanomaterials in the hydrogenation reaction of (E)-cinnamaldehyde (I), some tests were performed in the presence of isopropanol, using a substrate/MNP molar ratio of 1000/1 at 50 °C. During the reduction reaction, hydrogen atoms can be added across either the C=C or the C=O bonds to form hydrocinnamaldehyde (II), hydrocinnamic alcohol (III), or cinnamic alcohol (IV), respectively [30]. After the reduction reaction, compound II could react with isopropanol alcohol, affording the hemiacetal V (Table 1).

From a preliminary screening, it was found that the Hal@PDA/CuNP catalyst turned out to be not efficient in this kind of reaction, probably due to the leaching of metals from the support, as testified by the green supernatant solutions obtained after the first cycle, and thus it was no further considered. On the contrary, the Hal@PDA/PdNP nanomaterial showed good catalytic results, with satisfactory TOF values, as reported in Table 1, in line with, or in some case better than, those reported in the literature (Table 2). In all cases investigated, product IV was never produced.

Firstly, the catalyst with a PdNP content of ca. 3.6 wt% was tested at a temperature of 50 °C in the presence of 0.5 MPa of H_2 (entry 1). In this case, the catalyst proved to be very active, showing complete substrate conversion and a greater selectivity towards the saturated aldehyde (II), even if the hydrocinnamic alcohol (III) was formed at about 30%.

Table 1. Hydrogenation of (E)-cinnamaldehyde (I) catalyzed by Hal@PDA/PdNPs with different Pd content, using isopropanol as solvent and a substrate/Pd molar ratio = 1000/1.

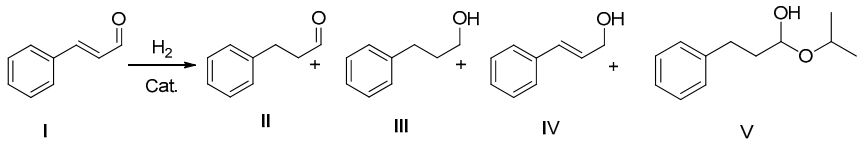

I II III IV V

Entry	P_{H_2} (MPa)	t (h)	Conv. (%) [a]	II Yield (%) [a]	III Yield (%) [a]	V Yield (%) [a]	TOF (s^{-1}) [c]
1 [b]	0.5	16	100	68	32	/	0.02
1 [b]*	0.5	16	100	69	31	/	
2	0.5	5	100	77	17	6	0.06
2 *	0.5	5	100	86	14	/	
2 **	0.5	5	100	86	14	/	
2 ***	0.5	5	100	80	13	7	
2 ****	0.5	5	100	83	9	8	
2 *****	0.5	5	99	83	10	6	
3	0.1	5	100	89	9	2	0.06
3 *	0.1	5	100	95	4	1	
4	0.1	3	69	54	7	8	0.06
4 *	0.1	3	100	91	3	6	0.1
4 **	0.1	3	100	96	3	1	
4 ***	0.1	3	100	91	6	3	

[a] Determined by GC analysis. Substrate (1.9 mmol); solvent: isopropanol (5 mL); substrate/Pd (molar ratio) = 1000/1. [b] Pd content in the catalyst: 3.6 wt%. [c] TOF = $n_p/n_c t$, where n_p and n_c are the moles of the product molecules and the catalyst during time t, respectively. * Experiment carried out by using the catalyst recovered from the previous reaction.

Table 2. Different metal-based catalysts for cinnamaldehyde hydrogenation.

Catalyst	TOF/s^{-1}	Ref.
Ru/CNTs	0.17	[31]
Ru/TEGO	0.033	[32]
Ir/GA	0.005	[33]
Au-PVP/SiO_2-12UVO	0.028	[34]
Pd/BP	0.014	[35]
Ni-CNT	0.0002	[36]
Pt/SiO_2	0.013	[37]
Pt-SnO_2/SiO_2	0.03	[37]
Hal@PDA/PdNPs	0.1	This work

This is not a surprising finding because it is well known that Pd-based catalysts preferentially hydrogenate the C=C double bond over the C=O one.

Noteworthily, both the activity and the selectivity remained practically unchanged in a recycling test (entry 1 [b]*).

To achieve more sustainable development, a Hal@PDA/PdNP nanomaterial with a lower PdNP content was prepared and tested in the hydrogenation reaction. In particular, the content of PdNPs in the nanomaterial was reduced from ca. 3.6 wt% to ca. 0.8 wt% (see Supplementary Materials), as estimated by TGA (Figure S1). By performing the reaction at 0.5 MPa of H_2 for 5 h, complete substrate conversion was achieved with the predominant formation of the saturated aldehyde (II) (entry 2). Recycling

tests showed that the Hal@PDA/PdNP catalyst retained both activity and selectivity for at least six consecutive runs (Table 1 and Figure 5). By reducing the H_2 pressure to 0.1 MPa, excellent results were obtained both in terms of activity and selectivity, even after one consecutive run (entries 3 and 3 *). By decreasing the reaction time from 5 h to 3 h, a decrease both in the conversion and in the selectivity towards the aldehyde (II) was observed (entry 4). Surprisingly, recycling tests showed that after the first run, the catalyst recovers its catalytic performance, affording a total conversion of (E)-cinnamaldehyde with high selectivity (greater than 90%) towards product (II). Most likely, after the first catalytic run, the catalyst underwent activation by hydrogen, remaining active and selective even in four consecutive runs (entries 4 *–4 ***).

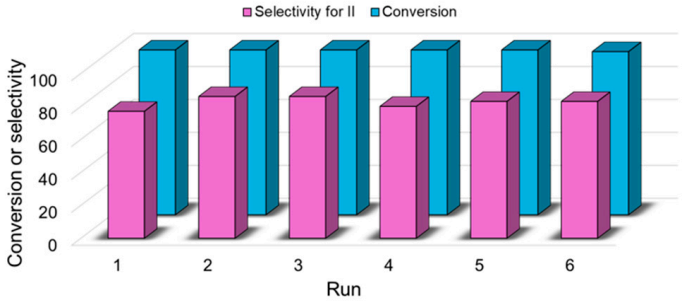

Figure 5. Conversion of (E)-cinnamaldehyde and its selectivity towards hydrocinnamaldehyde (II) after six consecutive runs.

As a matter of fact, palladium can be easily oxidized, by accidental contact with air, during the catalyst recovery operation. However, Pd(II) can be just as easily reduced back to active Pd(0) during the hydrogenation process.

Finally, the catalyst recovered after the first recycling test, and after five consecutive runs, it was subjected to XPS analysis, and the results were compared to those of Hal@PDA/PdNPs (Figures 2c and 6) in order to better understand the catalytic performance. As shown in Figure 6, the amount of Pd(0) slightly decreased after the first catalytic run (from 78% to 75%, Figure 6a), whereas it is strongly oxidized after five consecutive runs, where ca. 36% of Pd(0) was found by XPS analysis (Figure 6b). However, as shown by the catalytic tests (Table 1), the catalyst retains its catalytic activity and selectivity. Very probably, under the reaction conditions, hydrogen pressure can reactivate the catalyst, allowing it to keep its activity practically unchanged.

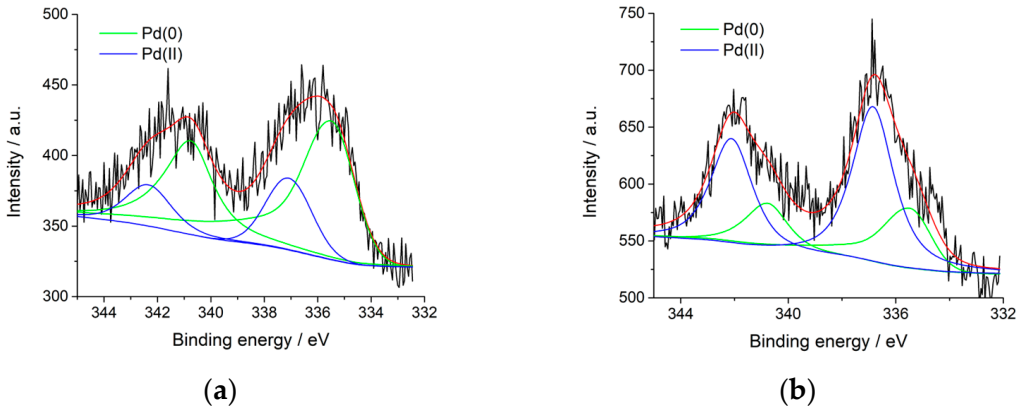

Figure 6. High-resolution X-ray photoelectron spectroscopy (XPS) of the Pd3d region of (**a**) after one and (**b**) five consecutive runs: Hal@PDA/PdNP nanomaterial.

2.2.2. 4-Nitrophenol Reduction

To further evaluate the catalytic performance of the Hal-based catalysts obtained, the reduction of 4-NP by $NaBH_4$ was studied, since this is the most frequently used reaction to investigate the catalytic activity of metal nanoparticles in aqueous solution. The interest in this reaction is mainly due to 4-NP being a common reactant in pharmaceuticals and the fact that it can be a hazardous byproduct that is inhibitory and toxic in nature; the product of the reaction, 4-aminophenol (4-AP), is used for black-and-white films and for the production of acetaminophen. By adding both catalysts to an aqueous solution of 4-NP in the presence of $NaBH_4$ (100 mM), the absorbance value at ca. 400 nm, typical of 4-nitrophenolate ions, decreases as a function of the time, and the solution color fades from yellow-green to transparent, indicating that both nanomaterials can exert catalytic activity. No change in the 4-NP absorbance was observed without the catalysts and in the presence of the Hal@PDA nanomaterial.

The reaction kinetics can be analyzed by plotting the absorbance value at 397 nm as a function of the time. Figure 7 shows plots of $\ln(A_t/A_0)$ versus reaction time, where A_t is the absorbance at reaction time t and A_0 is the initial absorbance. The results indicate that $\ln(A_t/A_0)$ decreases linearly with the reaction time, which is consistent with the pseudo-first-order kinetics of 4-NP reduction by $NaBH_4$, in a concentration-dependent manner.

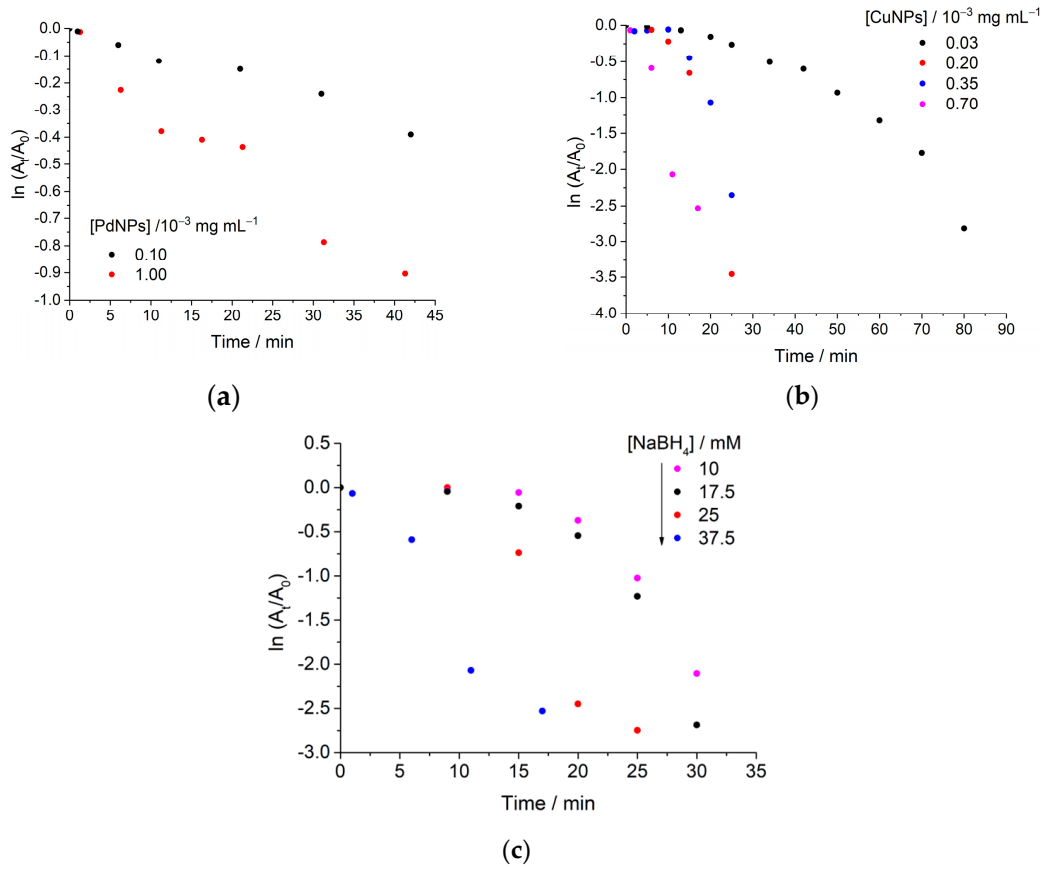

Figure 7. Plots of $\ln(A_t/A_0)$ versus time for various (**a**) Hal@PDA/PdNPs, (**b**) Hal@PDA/NPs, and (**c**) $NaBH_4$, in the presence of Hal@PDA/CuNP catalyst concentrations. The concentrations of 4-NP and NaBH4 in (**a**,**b**) are 0.050 mM and 25 mM, respectively. The concentrations of 4-NP and Hal@PDA/CuNPs in (**c**) are 0.050 mM and 0.1 mg mL^{-1} (corresponding to [CuNPs] = 0.7 × 10^{-3} mg mL^{-1}), respectively.

The apparent reaction time constant k_{app} (min^{-1}) was estimated by the linear fitting of the experimental results, and the data obtained are listed in Table 3.

Table 3. Kinetic parameters of 4-NP reduction at different Hal@PDA-based catalysts concentrations [a].

Entry	MNP Concentration/ $\times 10^{-3}$ mg mL^{-1}	$k_{app}/\times 10^{-3}$ min^{-1}
	Hal@PDA/PdNPs	
1	1.00	22
2	0.10	8
	Hal@PDA/CuNPs	
4	0.70	160
5	0.35	80
6	0.20	70
7	0.03	31

[a] Reaction conditions: 0.050 mM of 4-NP and 25 mM of $NaBH_4$.

As it is possible to observe from data reported in Table 3, the Hal@PDA/CuNP nanomaterial is shown to be most active in the reduction of 4-NP in the presence of $NaBH_4$. For this reason, further investigations were performed with this nanomaterial.

The actual kinetic constant (k) can be easily determined from the slope of a plot of k_{app} versus [$NaBH_4$]. Thus, the influence of $NaBH_4$ concentration on the reduction reaction was evaluated, and the obtained results are reported in Figure 7c, which shows that with increasing $NaBH_4$ concentration, an increase in the reaction rate occurs. The actual kinetic constant was calculated to be 0.003 min^{-1} (Figure S2).

Finally, to study the recyclability of the Hal@PDA/CuNP nanomaterial, the same catalyst was used to perform the same reduction reaction for consecutive runs. After each catalytic cycle, the catalyst (20 mg) was centrifuged, washed several times with water and dried for the next cycle of catalysis. The catalyst exhibits high activity in the same reaction time (30 min) after being used for eight cycles without presumably leaching CuNPs. XPS measurements on the catalyst after the recycling tests showed that the predominant species in the spent catalyst is the Cu^{2+} because of the presence of a peak centered at ca. 933.7 eV and the satellite one at ca. 943.4 eV (Figure 8).

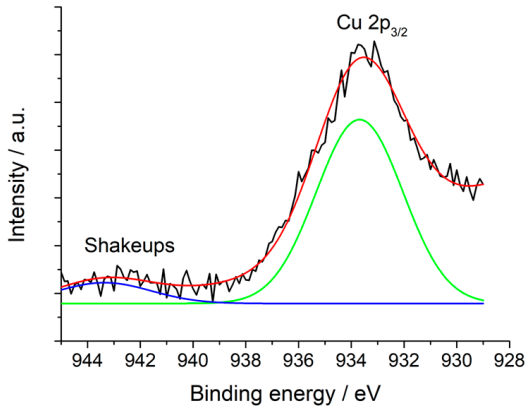

Figure 8. High-resolution X-ray photoelectron spectroscopy (XPS) of the Cu $2p_{3/2}$ region of the spent Hal@PDA/CuNP nanomaterial.

3. Materials and Methods

All reagents needed were used as purchased (Merck, Milan, Italy) without further purification.

Hal@PDA was synthetized as reported elsewhere [17].

3.1. General Procedure for the Synthesis of the Hal@PDA/PdNP Nanomaterial

$PdCl_2$ (4 mg, 0.023 mmol, 1 eq) and NaCl (27 mg, 0.46 mmol, 20 eq) in water (1 mL) were heated at 80 °C until the $PdCl_2$ was dissolved. The obtained clear reddish solution of sodium tetrachloropalladate (II) was cooled at room temperature and added dropwise to a suspension of Hal@PDA (50 mg) in water (2 mL). The suspension was left to stir at room temperature for 16 h and then filtered and washed several times with water to remove the unreacted materials. The solid obtained was re-suspended in ethanol (1 mL), and a solution of $NaBH_4$ (6 mg, 0.161 mmol, 7 eq) in ethanol (1 mL) was added dropwise to the obtained dispersion. The obtained dispersion was left to stir at room temperature for 6 h. After this time, the solvent was filtered off, and the powder was washed several times with water and then dried overnight at 60 °C. The amount of Pd in the nanomaterial was estimated by TGA to be as large as 3.6 wt%.

Using a similar procedure, but reducing the content of Pd salt and proportionally the amount of the other reagents, Hal@PDA/PdNPs with a content of 0.8 wt% of Pd catalyst were prepared (see Supplementary Materials).

3.2. General Procedure for the Synthesis of Hal@PDA/CuNP Nanomaterials

In a round-bottom flask, $CuCl_2$ (7 mg, 0.052 mmol) and Hal@PDA (50 mg) were weighed, and 2 mL of water was added. The suspension was left to stir at room temperature for 16 h and then filtered and washed several times with water to remove the unreacted materials. The solid obtained was re-suspended in ethanol (1 mL), and a solution of $NaBH_4$ (10 mg, 0.27 mmol) in ethanol (1 mL) was added dropwise to the obtained dispersion. The obtained dispersion was left to stir at room temperature for 6 h. After this time, the solvent was filtered off, and the powder was washed several times with water and then dried overnight at 60 °C. The amount of Cu in the nanomaterial was estimated by TGA to be as large as 0.6 wt%.

3.3. General Procedure for the Hydrogenation of Cinnamaldehyde (I)

In a 50 mL test tube, equipped with a magnetic stir bar, 1.9 mmol of cinnamaldehyde (I), 0.0019 mmol of Pd-based catalyst (substrate (I)/Pd molar ratio 1000/1), and 5 mL of isopropanol were added under an inert nitrogen atmosphere. The tube was then transferred into a 150 mL stainless steel autoclave under nitrogen, pressurized with hydrogen, and maintained under stirring at 50 °C for the due time (see Table 1 for the reaction conditions). The reactor was then cooled to room temperature, and the residual gases were released. The reaction mixture was centrifuged at 5000 rpm for 20 min: the solution was removed with a Pasteur pipette, and the solid was placed under a nitrogen flow until completely dry. The recovered catalyst was added to a solution of fresh substrate dissolved in 2-propanol and recycled by adopting the procedure described above. The organic phase was analyzed by GC and GC-MS.

GC-MS m/z 3-Phenyl propanal (II): 134 $[M]^+$; 105 $[M-CHO]^+$; 91 $[M-C_2H_3O]^+$; 78 $[M-C_3H_4O]^+$.

GC-MS m/z Hydrocinnamic alcohol (III): 136 $[M]^+$; 118 $[M-H_2O]^+$; 105 $[M-CH_2OH]^+$; 91 $[M-C_2H_5O]^+$; 77 $[M-C_3H_7O]^+$.

3.4. 4-NP Reduction Reaction

Hal@PDA/PdNP or Hal@PDA/CuNP aqueous suspension (different volumes to reach the desired catalyst amount) was added into a mixed aqueous solution of 2 mL containing 4-NP (0.05 mM) and $NaBH_4$ (from 10 to 37.5 mM) in a quartz cuvette, at room temperature and under stirring. The reduction process was monitored by recording the UV–vis spectra of the reaction mixture at different times. The reaction rate constant was

determined by measuring the absorption intensity of the initially observed peak of the substrate as a function of the time.

3.5. Recyclability of Hal@PDA/CuNP Catalysts

Hal@PDA/CuNPs (20 mg), 4-NP (0.010 mM), and $NaBH_4$ (25 mM) were placed in a vial under constant stirring and at room temperature. After 30 min, the complete reduction was confirmed by measuring the absorption intensity at 397 nm. The reaction mixture was then centrifuged, and the supernatant was decanted; the residual solid was washed three times with water. The Hal@PDA/CuNP nanomaterials were dried and reused in the same reaction for ten consecutive cycles.

4. Conclusions

In summary, two hybrid nanomaterials were developed by immobilizing palladium or copper nanoparticles onto halloysite nanotubes (Hal) selectively functionalized with polydopamine (PDA). Building upon our previously reported ZnO-assisted, site-specific PDA functionalization strategy, this work demonstrates its versatility as a robust and tunable platform for the controlled immobilization of different metal nanoparticles. The resulting materials, Hal@PDA/PdNPs and Hal@PDA/CuNPs, display uniformly distributed ultrasmall nanoparticles (<5 nm) with strong surface interaction and long-term catalytic stability, representing a significant step toward the design of sustainable and recyclable hybrid catalysts.

The amount of immobilized metal NPs on the support was estimated by TGA to be ca. 3.6 wt% and 0.7 wt% for PdNPs and CuNPs, respectively. Their performance in two model reactions, (E)-cinnamaldehyde hydrogenation and 4-nitrophenol reduction, showed distinct and complementary catalytic behavior, with both systems maintaining recyclability under the tested conditions.

Regarding cinnamaldehyde reduction, this reaction was performed in the presence of isopropanol using the substrate/MNP molar ratio of 1000/1 at 50 °C, varying the reaction time and H_2 pressure. The results showed that the Hal@PDA/PdNP nanomaterial provided good catalytic performance, with satisfactory TOF values comparable with the literature. It showed high catalytic activity and selectivity toward hydrocinnamaldehyde even after six consecutive cycles. X-ray photoelectronic spectroscopy (XPS) on fresh and spent catalyst demonstrated that after six consecutive cycles, PdNPs on Hal@PDA/PdNPs were strongly oxidated. Despite this, the catalyst retained its catalytic activity and selectivity. Very probably, under the reaction conditions, hydrogen pressure can reactivate the catalyst, allowing it to keep its activity practically unchanged.

Conversely, although both catalysts show catalytic activity in 4-nitrophenol reduction, the most promising one is found to be the Hal@PDA/CuNP nanomaterial, which shows increasing catalytic activity by increasing $NaBH_4$ and nanomaterial concentration. Recycling tests show that the catalyst can be used without any loss of catalytic activity for at least eight consecutive cycles. These findings highlight the effectiveness of site-selective PDA functionalization in stabilizing metal nanoparticles and establish Hal@PDA as a versatile and tunable platform for the design of next-generation hybrid nanomaterials.

Supplementary Materials: The following supporting information can be downloaded at https://www.mdpi.com/article/10.3390/catal15111029/s1, Instrumentation used, Synthesis of HNTs@PDA/PdNPs nanomaterial, Figure S1: Thermogravimetric curve of Hal@PDA and Hal@PDA/PdNPs nanomaterials, Figure S2: Conversion of (E)-cinnamaldehyde and its selectivity towards hydrocinnamaldehyde (II) after six consecutive runs, Figure S3: High-resolution X-ray photoelectron spectroscopy (XPS) of the Pd3d region of (a) after first and (b) five consecutive runs, Hal@PDA/PdNPs nano-

material, Figure S4: Plot of kapp versus [NaBH4], Figure S5: XPS survey of the Hal@PDA/CuNPs nanomaterial, Table S1. Comparison of dimensions and application of the developed catalysts.

Author Contributions: Conceptualization, S.P. and S.R.; methodology, M.M., C.D., M.L.A., L.F.L., A.L.-G., R.d.M.B., O.P. and R.S.-E.; formal analysis, M.M., S.P., M.L.A., L.F.L., A.L.-G., R.S.-E., C.V. and S.R.; investigation, M.M., C.D., S.P., L.F.L., A.L.-G. and S.R.; resources, C.V.; writing—original draft, M.M., S.P., L.F.L. and S.R.; writing—review and editing, M.M., S.P., O.P. and S.R. All authors have read and agreed to the published version of the manuscript.

Funding: This work was supported by Linea di Intervento 1 Progetti di Ricerca Collaborativa del "PIAno di inCEntivi per la RIcerca di Ateneo 2024/2026" of University of Catania with the project "Sviluppo di nanobiopesticidi basati su argille minerali per applicazioni in agricoltura".

Data Availability Statement: The raw data supporting the conclusions of this article will be made available by the authors on request.

Acknowledgments: ATeN Center–University of Palermo is acknowledged for providing XPS measurements.

Conflicts of Interest: The authors declare no conflicts of interest.

References

1. Ying, S.; Guan, Z.; Ofoegbu, P.C.; Clubb, P.; Rico, C.; He, F.; Hong, J. Green synthesis of nanoparticles: Current developments and limitations. *Environ. Technol. Innov.* **2022**, *26*, 102336. [CrossRef]
2. Fan, W.K.; Tahir, M. Structured clay minerals-based nanomaterials for sustainable photo/thermal carbon dioxide conversion to cleaner fuels: A critical review. *Sci. Total Environ.* **2022**, *845*, 157206. [CrossRef] [PubMed]
3. Calvino, M.M.; Lisuzzo, L.; Cavallaro, G.; Lazzara, G.; Yadav, R.P.; Dolgan, K.; Lvov, Y.M. The Emerging Role of Halloysite Clay Nanotube Formulations in Cosmetics and Topical Drug Delivery. *ACS Appl. Bio Mater.* **2025**, *8*, 2674–2690. [CrossRef] [PubMed]
4. Das, S.; Jana, S. A tubular nanoreactor directing the formation of in situ iron oxide nanorods with superior photocatalytic activity. *Environ. Sci. Nano* **2017**, *4*, 596–603. [CrossRef]
5. Stavitskaya, A.; Rubtsova, M.; Glotov, A.; Vinokurov, V.; Vutolkina, A.; Fakhrullin, R.; Lvov, Y. Architectural design of core–shell nanotube systems based on aluminosilicate clay. *Nanoscale Adv.* **2022**, *4*, 2823–2835. [CrossRef] [PubMed]
6. Stavitskaya, A.; Glotov, A.; Pouresmaeil, F.; Potapenko, K.; Sitmukhanova, E.; Mazurova, K.; Ivanov, E.; Kozlova, E.; Vinokurov, V.; Lvov, Y. CdS Quantum Dots in Hierarchical Mesoporous Silica Templated on Clay Nanotubes: Implications for Photocatalytic Hydrogen Production. *ACS Appl. Nano Mater.* **2022**, *5*, 605–614. [CrossRef]
7. Yaghoubi, S.; Sadjadi, S.; Zhong, X.; Yuan, P.; Heravi, M.M. Clay-supported bio-based Lewis acid ionic liquid as a potent catalyst for the dehydration of fructose to 5-hydroxymthylfurfural. *Sci. Rep.* **2024**, *14*, 82. [CrossRef]
8. Casiello, M.; Savino, S.; Massaro, M.; Liotta, L.F.; Nicotra, G.; Pastore, C.; Fusco, C.; Monopoli, A.; D'Accolti, L.; Nacci, A.; et al. Multifunctional halloysite and hectorite catalysts for effective transformation of biomass to biodiesel. *Appl. Clay Sci.* **2023**, *242*, 107048. [CrossRef]
9. Lin, H.; Liu, Y.; Hu, C.; Deng, X.; Zhang, L.; Chen, S.; Zhang, H. Catalytic Nano-Gold Immobilized on the Inner Surfaces of Halloysite Nanotubes for Selective Reduction of Nitroaromatics. *ACS Appl. Nano Mater.* **2024**, *7*, 16669–16678. [CrossRef]
10. Zhou, T.; Liu, Z.; Kim, K.; Yu, T. Natural halloysite nanotubes enclosing PdAg alloy nanoparticles as nanoreactors with enhanced catalytic performance. *J. Colloid Interface Sci.* **2025**, *700*, 138531. [CrossRef]
11. Glotov, A.; Vutolkina, A.; Pimerzin, A.; Vinokurov, V.; Lvov, Y. Clay nanotube-metal core/shell catalysts for hydroprocesses. *Chem. Soc. Rev.* **2021**, *50*, 9240–9277. [CrossRef]
12. Lan, Y.; Ma, Y.; Hou, Q.; Luo, Z.; Wang, L.; Ran, M.; Dai, T. Immobilization of palladium nanoparticles on polydopamine spheres with superior activity and reusability in Heck reaction. *J. Catal.* **2024**, *430*, 115333. [CrossRef]
13. Liu, Y.; Ai, K.; Lu, L. Polydopamine and Its Derivative Materials: Synthesis and Promising Applications in Energy, Environmental, and Biomedical Fields. *Chem. Rev.* **2014**, *114*, 5057–5115. [CrossRef]
14. Zhang, D.; Cui, Y.; Yang, G.; Liu, M.; Zhu, G.; Sheng, X.; Deng, F.; Zhou, N.; Zhang, X.; Wei, Y. Mussel-inspired fabrication of halloysite nanotube-based magnetic composites as catalysts for highly efficient degradation of organic dyes. *Appl. Clay Sci.* **2020**, *198*, 105835. [CrossRef]
15. Liu, J. Catalysis by Supported Single Metal Atoms. *ACS Catal.* **2017**, *7*, 34–59. [CrossRef]

16. Massaro, M.; Casiello, M.; D'Accolti, L.; Lazzara, G.; Nacci, A.; Nicotra, G.; Noto, R.; Pettignano, A.; Spinella, C.; Riela, S. One-pot synthesis of ZnO nanoparticles supported on halloysite nanotubes for catalytic applications. *Appl. Clay Sci.* **2020**, *189*, 105527. [CrossRef]
17. Alfieri, M.L.; Massaro, M.; d'Ischia, M.; D'Errico, G.; Gallucci, N.; Gruttadauria, M.; Licciardi, M.; Liotta, L.F.; Nicotra, G.; Sfuncia, G.; et al. Site-specific halloysite functionalization by polydopamine: A new synthetic route for potential near infrared-activated delivery system. *J. Colloid Interface Sci.* **2022**, *606*, 1779–1791. [CrossRef]
18. Falanga, A.P.; Massaro, M.; Borbone, N.; Notarbartolo, M.; Piccialli, G.; Liotta, L.F.; Sanchez-Espejo, R.; Viseras Iborra, C.; Raymo, F.M.; Oliviero, G.; et al. Carrier capability of halloysite nanotubes for the intracellular delivery of antisense PNA targeting mRNA of neuroglobin gene. *J. Colloid Interface Sci.* **2024**, *663*, 9–20. [CrossRef]
19. Yi, F.; DeLisio, J.B.; Nguyen, N.; Zachariah, M.R.; LaVan, D.A. High heating rate decomposition dynamics of copper oxide by nanocalorimetry-coupled time-of-flight mass spectrometry. *Chem. Phys. Lett.* **2017**, *689*, 26–29. [CrossRef]
20. Zheng, C.; Cao, J.; Zhang, Y.; Zhao, H. Insight into the Oxidation Mechanism of a Cu-Based Oxygen Carrier (Cu → Cu2O → CuO) in Chemical Looping Combustion. *Energy Fuels* **2020**, *34*, 8718–8725. [CrossRef]
21. Gil, S.; Garcia-Vargas, J.M.; Liotta, L.F.; Pantaleo, G.; Ousmane, M.; Retailleau, L.; Giroir-Fendler, A. Catalytic Oxidation of Propene over Pd Catalysts Supported on CeO_2, TiO_2, Al_2O_3 and M/Al_2O_3 Oxides (M = Ce, Ti, Fe, Mn). *Catalysts* **2015**, *5*, 671–689. [CrossRef]
22. Massaro, M.; Borrego-Sánchez, A.; Sánchez-Espejo, R.; Viseras Iborra, C.; Cavallaro, G.; García-Villén, F.; Guernelli, S.; Lazzara, G.; Miele, D.; Sainz-Díaz, C.I.; et al. Ciprofloxacin carrier systems based on hectorite/halloysite hybrid hydrogels for potential wound healing applications. *Appl. Clay Sci.* **2021**, *215*, 106310. [CrossRef]
23. Al Abdullah, K.; Awad, S.; Zaraket, J.; Salame, C. Synthesis of ZnO Nanopowders By Using Sol-Gel and Studying Their Structural and Electrical Properties at Different Temperature. *Energy Procedia* **2017**, *119*, 565–570. [CrossRef]
24. Wojcieszak, R.; Genet, M.J.; Eloy, P.; Ruiz, P.; Gaigneaux, E.M. Determination of the Size of Supported Pd Nanoparticles by X-ray Photoelectron Spectroscopy. Comparison with X-ray Diffraction, Transmission Electron Microscopy, and H2 Chemisorption Methods. *J. Phys. Chem. C* **2010**, *114*, 16677–16684. [CrossRef]
25. Zhang, J.; Zhang, X.; Sun, H.; Shi, L.; Wei, J.; Xu, D.; Zhang, S.; Zhang, J.; Wang, S.; Sun, H. Uncovering catalytic activity of Cu species on boron/nitrogen co–doped carbon nanotubes for efficient hydrogenation of nitroaromatics: Beyond the size of metal active center. *Compos. Part B Eng.* **2025**, *293*, 112112. [CrossRef]
26. Sanakal, S.I.; Das, A.; Babu, A.; Kar, P.; Nutalapati, V.; Datta, K.K.R.; Banerjee, S.; Maji, S. Alginate-aminoclay/CuO nanocomposite beads: A sustainable and green approach for catalytic reduction of toxic nitroaromatic compounds. *J. Environ. Chem. Eng.* **2025**, *13*, 115398. [CrossRef]
27. Xu, X.; Ma, J.; Kui, B.; Zhu, G.; Jia, G.; Wu, F.; Gao, P.; Ye, W. Effect of Crystal Planes of Pd and the Structure of Interfacial Water on the Electrocatalytic Hydrogenation of Alkynes to Alkenes. *ACS Appl. Nano Mater.* **2023**, *6*, 5357–5364. [CrossRef]
28. Sahiner, M.; Demirci, S.; Sahiner, N. Enhanced Bioactive Properties of Halloysite Nanotubes via Polydopamine Coating. *Polymers* **2022**, *14*, 4346. [CrossRef]
29. Wang, X.; Liang, X.; Geng, P.; Li, Q. Recent Advances in Selective Hydrogenation of Cinnamaldehyde over Supported Metal-Based Catalysts. *ACS Catal.* **2020**, *10*, 2395–2412. [CrossRef]
30. Patil, K.N.; Manikanta, P.; Srinivasappa, P.M.; Jadhav, A.H.; Nagaraja, B.M. State-of-the-art and perspectives in transition metal-based heterogeneous catalysis for selective hydrogenation of cinnamaldehyde. *J. Environ. Chem. Eng.* **2023**, *11*, 109168. [CrossRef]
31. Wang, Y.; Rong, Z.; Wang, Y.; Zhang, P.; Wang, Y.; Qu, J. Ruthenium nanoparticles loaded on multiwalled carbon nanotubes for liquid-phase hydrogenation of fine chemicals: An exploration of confinement effect. *J. Catal.* **2015**, *329*, 95–106. [CrossRef]
32. Wang, Y.; Rong, Z.; Wang, Y.; Qu, J. Ruthenium nanoparticles loaded on functionalized graphene for liquid-phase hydrogenation of fine chemicals: Comparison with carbon nanotube. *J. Catal.* **2016**, *333*, 8–16. [CrossRef]
33. Li, L.; Gao, G.; Zheng, J.; Shi, X.; Liu, Z. Three-dimensional graphene aerogel supported Ir nanocomposite as a highly efficient catalyst for chemoselective cinnamaldehyde hydrogenation. *Diam. Relat. Mater.* **2019**, *91*, 272–282. [CrossRef]
34. Zhong, R.-Y.; Sun, K.-Q.; Hong, Y.-C.; Xu, B.-Q. Impacts of Organic Stabilizers on Catalysis of Au Nanoparticles from Colloidal Preparation. *ACS Catal.* **2014**, *4*, 3982–3993. [CrossRef]
35. Fujiwara, S.; Takanashi, N.; Nishiyabu, R.; Kubo, Y. Boronate microparticle-supported nano-palladium and nano-gold catalysts for chemoselective hydrogenation of cinnamaldehyde in environmentally preferable solvents. *Green Chem.* **2014**, *16*, 3230–3236. [CrossRef]

36. Patil, K.N.; Manikanta, P.; Srinivasappa, P.M.; Jadhav, A.H.; Nagaraja, B.M. Exploring the confined space and active sites of Ni@OCNTs catalyst for chemoselective hydrogenation of cinnamaldehyde to hydrocinnamaldehyde. *J. Environ. Chem. Eng.* **2022**, *10*, 108208. [CrossRef]
37. Wang, S.; Wu, B.; Zhang, Q.; Li, Y.; Zhu, L.; Yu, H.; Yin, H. Design of Pt@Sn core–shell nanocatalysts for highly selective hydrogenation of cinnamaldehyde to prepare cinnamyl alcohol. *Chem. Eng. J.* **2024**, *488*, 151019. [CrossRef]